

1 Using spatial patterns of fluvial incision to constrain 2 continental-scale uplift in the Andes.

3
4 L.A. Evenstar¹, A.E. Mather² and A.J. Hartley³

5
6 ¹School of Environment and Technology, University of Brighton, UK,

7 ²Department of Geography, Earth and Environmental Sciences, University of
8 Plymouth, UK,

9 ³Department of Geology and Petroleum Geology, University of Aberdeen, Aberdeen,
10 UK,

11 12 **Abstract**

13
14 Geomorphic archives, particularly longitudinal river profiles, are increasingly used as
15 a proxy to reconstruct uplift rates in mountainous regions. Within the Atacama
16 Desert, Northern Chile, slow, long-term erosion creates exceptional preservation of
17 fluvial and alluvial surfaces. This enables river incision patterns to be used on a
18 continental-scale (>250 km) along the western margin of the Andes (18°00'S to
19 20°15'S) and over a time frame from Miocene to Present day. The data show marked
20 compartmentalisation of fluvial system behaviour with changes in incision rates from
21 south to north creating 3 distinctly different regions. Within these different sectors,
22 incision rates are broadly consistent between rivers suggesting a regional rather than
23 a river specific control on rates. In Sector 1 (18°05'S to 19°20'S) the fluvial systems
24 are exorheic with a terminal base level (the lowest base level to which the river
25 system can erode) in the Pacific Ocean and span the Coastal Cordillera, Longitudinal
26 Valley, Precordillera and western edge of the Western Cordillera. This constrains the
27 total uplift over these regions to a minimum of 1200 m in 11 Myr with incision rates of
28 ~200-120 m/Myr consistent with rapid but sustained uplift of the Andes in the Late
29 Miocene. In Sector 2 (19°20'S to 19°50'S), to the immediate south, the rivers are
30 shorter and terminate in the Longitudinal Valley, spanning only the Longitudinal
31 Valley, Precordillera and the western edge of the Western Cordillera with lower
32 incision rates of 100-50 m/Myr. Comparison of incision rates between Sector 1 and 2
33 can constrain the uplift of the Coastal Cordillera to 60m/Myr which is in keeping with
34 previous studies from the region. In southernmost Sector 3 (19°50'S to 20°10'S), the
35 fluvial systems terminate in the Longitudinal Valley and span only the Longitudinal
36 Valley and eastern part of the Precordillera with low incision rates of 50 to 25 m/Myr.

37 Differences between Sectors 2 and 3 are attributable to drainage loss by tectonic
38 beheading of catchments through uplift of the Cordillera de Domeyko fault system,
39 placing a minimum constrain on uplift in this region of 50 to 25 m/Myr. This study
40 demonstrates the applicability of large-scale fluvial archives to access not just the
41 timing of uplift on a continental scale, but also the relative uplift of individual tectonic
42 provinces.

43

44 Keywords; Andes; Paleosurface; Atacama; Desert Pavement; landscape evolution;
45 climate; base levels; fluvial incision, fluvial archives, terraces.

46

47 **1. Introduction**

48

49 Fluvial geomorphological archives are being increasingly used to reconstruct climate
50 and deformation (e.g. Macklin et al., 2002, Bridgeland et al., 2012, Stokes et al.
51 2017, Evenstar et al. 2018; Stokes et al., 2018). These archives comprise dominantly
52 erosional (e.g strath terrace) through to depositional records (e.g. distributive fluvial
53 systems) and can be regionally extensive (e.g. pediment systems). The common
54 theme is that these types of geomorphic archive have low angle surface expressions
55 which can be reconstructed to enable surface deformation to be quantified (e.g.
56 Gesch et al., 2014; Demoulin et al 2017, Stokes et al., 2018). Typically the majority of
57 these studies concentrate on a single pediment surface over small basin scale or
58 focus on trunk drainage or tributaries along a single river system (e.g. Anton et al.,
59 2014, Martins et al., 2017, Evenstar et al., 2018). Whilst correlation of fluvial system
60 behaviour has been attempted across regional scales (>100's km) to examine
61 climate controls (e.g. Macklin et al, 2002), flooding records (e.g. Benito et al., 2000)
62 and uplift rates (Litchfield and Berryman 2006) this has typically been restricted to
63 time-scales younger than the Pliocene. The few studies that look at regional scale
64 deformation over longer timescales tend to utilise modelling of profiles or terrace
65 patterns due to limited preservation of the fluvial system (e.g. Demoulin et al., 2007,
66 Boulton et al., 2014). Where appropriate records are well preserved (e.g. in arid
67 landscapes), availability of high-resolution satellite data sets facilitate regional
68 geomorphic reconstruction over much wider spatial and temporal scales than was
69 previously possible.

70

71 The Atacama is the most arid and potentially, oldest desert region in the world
72 (Hartley et al., 2005, Dunai et al., 2005). The long term sustained arid climate leads
73 to preservation of ancient landscapes, some of which are dated back to the Late

74 Oligocene (Dunai et al. 2005, Evenstar et al. 2009, Evenstar et al. 2017). Several of
75 these surfaces are identified as being generated following abandonment of fluvial
76 incision events associated with fluctuating climate and long-term uplift of the Andean
77 mountain chain (Evenstar et al. 2017). Within hyper-arid fluvial systems, as a function
78 of their low geomorphic erosional efficiency, even modest vertical crustal uplift is
79 likely to be more directly expressed as surface uplift, and thus more likely to be
80 recorded within fluvial archives (e.g. Demoulin et al., 2017). In the central Andes
81 (Atacama Desert) the sustained dominance of extreme aridity is expressed by the
82 presence of near linear to convex hypsometric curves that are typical of areas
83 experiencing ineffective fluvial incision (Montgomery et al., 2002). This incision, in
84 response to tectonic uplift, is documented in the fluvial archives, and along with the
85 past climate (e.g. Dunai et al., 2005; Evenstar et al., 2009; Evenstar et al., 2017),
86 these fluvial archives are increasingly well understood (Victor et al., 2004, Fariás et
87 al., 2005, Jordan et al., 2014, van Zalinge et al., 2017) and can be exploited to
88 examine continental scale uplift. These approaches have documented vastly different
89 rates of fluvial incision in northern Chile from 100 m/m.y. (Hoke et al., 2007) to 10
90 m/m.y (Cooper et al., 2016) since the Middle Miocene leading to different models for
91 timing of Andean uplift.

92
93 Here, we utilise freely available satellite remotely sensed data, together with longer
94 term geological and geomorphological erosional and depositional records to
95 reconstruct and quantify the last 11 Myr of pediment and fluvial landscape erosion
96 along the western side of the Central Andes orogen, a classic subduction zone
97 setting. The low erosional efficiency of this landscape means that the surface uplift is
98 preserved in excellent detail. The present study seeks to establish a continental scale
99 view of the fluvial incision and how this varies parallel to the Andean Mountain chain.
100 Using this we aim to establish the main controlling factors on incision rates in order to
101 better understand their use in constraining continental scale uplift within the Central
102 Andes.

103

104 **2. Study area: landscape components and depositional record**

105 The study region runs along the western margin of the Central Andean mountain
106 range from 18°00'S to 20°15'S (Figure 1a). This region consists of several different
107 morphotectonic provinces; the Coastal Cordillera, Longitudinal Valley, Precordillera
108 and Western Cordillera (Figure 1a). The Coastal Cordillera runs along the coast of
109 the Pacific Ocean and is characterised by the eroded Jurassic magmatic arc. The
110 Coastal Cordillera is absent around the border between Chile and Peru (18°30'S) but

111 increases in width and height towards the south (Madella et al., 2017). The Coastal
112 Cordillera shows exhumation back to the Eocene (Juez-Larre et al., 2010). However
113 the timing of uplift of this range is poorly constrained with rates varying from
114 0.001mm/yr to 0.1 mm/yr proximal to the coast (Regard et al. 2010; Garcia-Perez et
115 al., 2018) to 0.05 mm/yr to 0.07 mm/yr inland (Hartley et al., 2000; Dunai et al., 2005;
116 Cosentino and Jordan 2017). On the regional scale the mountain range was still at or
117 close to sea level in the Late Oligocene forming the regionally extensive Tarapaca
118 surface that graded down to sea level (Noble et al., 1985, Delouis et al., 1998, Dunai
119 et al., 2005; Thouret et al., 2007). The mountain range is believed to have uplifted
120 continuously from the late Oligocene at an average rate of 0.05 mm/yr to 0.07 mm/yr
121 (Delouis et al., 1998; Hartley et al., 2000; Dunai et al., 2005; Cosentino and Jordan
122 2017). To the east, the Coastal Cordillera borders the Longitudinal Valley, a deep
123 fore arc basin infilled with Oligocene to Miocene aged sediments derived from the
124 Andean mountain range to the east (Evenstar et al., 2009; Hartley & Evenstar 2010).
125 The top of the basin is characterized by an elevated low-relief relict landscape
126 termed the Pacific Paleosurface (PPS) (Evenstar et al., 2017). The Longitudinal
127 Valley is characterized by a series of westward propagating reverse faults or
128 monocline folds which have been active from ~30 to 5 Ma (Victor et al., 2004, Garcia
129 2005, Farías et al., 2004). To the east of the Longitudinal Valley lies the
130 Precordillera. This rises in elevation from 2000 to 4000 masl and is characterized by
131 a series of westward propagating, north-south striking thrusts and folds related to the
132 Domeyko fault system (Figure 1). The Precordillera forms the foothills to the modern
133 magmatic arc in the east, termed the Western Cordillera with peaks up to 6000 m.
134
135 The Precordillera and Longitudinal Valley are infilled by volcanoclastic and fluvial
136 sediments, which were predominantly deposited syn-tectonically (Figure 2). The oldest
137 sediments in the region are the Azapa Formation, a series of alluvial conglomerates
138 dated at ~35 to 22.7 Ma (Wörner et al., 2000; Wotzlaw et al., 2011; van Zalinge et.,
139 2017). Overlying the Azapa Formation in the Longitudinal Valley, and unconformably
140 overlying the basement in the Precordillera, are a series of ignimbrites and
141 volcanoclastic sediments termed the Oxaya Formation (22.7 Ma -19.7 Ma) (Wörner et
142 al., 2000; van Zalinge et., 2017). North of 19°00'S, these deposits are predominantly
143 formed by thick ignimbrite sheets (up to 1000 m) (van Zalinge et al., 2017). In the
144 area around the Lluta Quebrada, the ignimbrite sequence forms the top of the
145 stratigraphic succession in the Longitudinal Valley (Figure 2 and 3). In contrast,
146 towards the south, the ignimbrite sheets thin and are intercalated with more fluvial
147 sediments (Hartley and Evenstar, 2010). South of Quebrada Lluta, the volcanoclastic

148 sediments in the Longitudinal Valley are conformably overlain by the El Diablo
149 Formation (Figure 2), a series of fluvial sediments dated at 16 -11 Ma (Evenstar et
150 al., 2017). Within this region the El Diablo Formation is overlain by the Tana lava
151 dated at 8.8 ± 0.5 Ma (Mortimer et al., 1974) and 8.2 ± 0.5 Ma (Muñoz and
152 Sepulveda, 1992) constraining the age of the end of the El Diablo Formation to 11-8
153 Ma.

154

155 This study focuses on the PPS which is formed from numerous distributive fluvial
156 systems, which can be found in the Longitudinal Valley and in parts of the
157 Precordillera (Evenstar et al., 2017). North of $19^{\circ}20'S$, the PPS is deeply dissected
158 (up to 1,700 masl) by five main rivers (Lluta, Azapa, Victor, Camarones and Tana)
159 that drain to the Pacific Ocean (exorheicly drained) with a terminal base level of 0
160 masl (Fig. 1). Analysis of the fluvial profiles of Quebrada Tana shows that the main
161 knickpoint is within the Coastal Cordillera (Garcia et al., 2011; Evenstar et al., 2017;
162 Kirk-Lawlor et al., 2013), suggesting that it has not yet adapted to the new terminal (0
163 masl) base level, with the upper reaches of the river still grading down to the former
164 terminal base level within the Longitudinal Valley at 1000 masl (Kirk-Lawlor et al.,
165 2013; Evenstar et al., 2017). The timing of when fluvial regions north of Quebrada
166 Tana became exorheicly drained is considered to be diachronous from the Early to
167 Mid Miocene (Evenstar et al., 2017). South of this region, the main rivers (Aroma,
168 Tarapaca, de Parca and Tambillo) terminate within the Longitudinal Valley
169 (endorheicly drained) with terminal base levels of ~ 1000 masl and incise the PPS
170 towards the Western Cordillera by up to 1000 masl (Hoke et al., 2007).

171

172 The PPS can be traced for over 600 km (south to north) within the Longitudinal
173 Valley. The surface has been mapped in detail using remote sensing techniques and
174 constrained in age using cosmogenic isotope dating techniques in Evenstar et al.,
175 (2017). This research demonstrates that the PPS is in fact formed from an
176 amalgamation of geomorphic surfaces (both erosional (inset) and depositional
177 (overlying)) spanning a range of ages from the Late Oligocene to present day
178 (Evenstar et al., 2009; 2017). The timing of formation of the surface is related to
179 regional climate while the geographical location of the individual components that
180 comprise the surface are controlled by regional tectonic activity (Evenstar et al.,
181 2017). Within the present study we examine the youngest three geomorphic
182 surfaces; Aggradational Surface 4 (AS4), Degradational Surface 3 (DS3) and
183 Degradational Surface 2 (DS2) (Terminology after Evenstar et al., 2017 and shown in
184 Figure 2 and 3). Aggradational surface 4 (AS4) represents the end of deposition of

185 the El Diablo formation and is dated at 11 Ma using *insitu* exposure ages (Evenstar
186 et al., 2017). Degradational surface 3 (DS3) is an erosion system which cuts into the
187 underlying sediment fill of the basin (El Diablo Formation and Oxaya Formation). The
188 surface comprises a relict dendritic drainage pattern abandoned at ~7 Ma (*insitu*
189 exposure ages, Evenstar et al., 2017). Degradational System 2 (DS2) cuts into the
190 older geomorphic surface DS3 and is characterized by a trellis drainage pattern. The
191 abandonment of this surface is constrained at ~3 Ma (Evenstar et al., 2017). Along
192 the Quebrada Lluta, lies a large (26 km³) landslip deposit, the Lluta collapse, which
193 disrupts various surfaces. This feature shows westward collapse into the Longitudinal
194 Valley and is believed to have formed at ~3 Ma (Wörner et al., 2002; Kober et al.,
195 2007; Evenstar et al., 2017).

196

197 The timing and rate of uplift of the Andes is still ambiguous, with two favoured end-
198 member models (Fig. 2); (1) rapid, late Miocene uplift, with surface uplift of ~2.5 km
199 between 11 and 6 Ma (e.g. Garzzone et al., 2006; Ghosh et al., 2006, Garzzone et al.,
200 2008); and (2) slow and steady uplift that started in the late Eocene (e.g. Victor et al.,
201 2004; Hartley et al., 2007; Barnes and Ehlers, 2009; Evenstar et al., 2015; van
202 Zalinge et al., 2017). Thus, the eastern edge of the PSS has experienced substantial
203 cumulative surface uplift regardless of which model is taken throughout the Miocene
204 and Pliocene. Several studies have used the main fluvial systems in the region to
205 calculate regional uplift of the Andes across the region (e.g. Farías et al., 2005, Hoke
206 et al., 2007; Schildgen et al., 2002; Schildgen et al., 2009). However, more recent
207 climate modelling of this region has cast doubt on this interpretation suggesting
208 higher incision rates could be due to increased orographically generated precipitation
209 (Ehlers and Poulsen, 2009).

210

211 Along the western margin of the Andes, the PSS has been undergoing uplift since at
212 least the Early Miocene (Evenstar et al., 2015) and likely extends back further to the
213 early Oligocene (Barnes and Ehler 2009, van Zalinge et al., 2017). The uplift of the
214 region is modified locally predominantly north-south fault systems (Figure 1) (Wörner
215 et al. 2002; Victor et al. 2005; Farías et al. 2005; van Zalinge et al. 2017) with minor
216 amounts of surface uplift expressed as regional tilting (Farías et al. 2005). However,
217 there are no marked changes in regional tectonic uplift from North to South over the
218 study area with similar rates and timing of uplift (2500m to 3200m of uplift during 25
219 Ma to 8 Ma) reported from 18°S to 22°S in Northernmost Chile by numerous authors
220 (Wörner et al., 2002; Victor et al., 2005; Farías et al., 2005; Jordan et al., 2014;
221 Evenstar et al., 2015; van Zalinge et al., 2017).

222

223 **3. Study area climate**

224 The past climate of the region is reasonably well constrained (Fig. 2). The climate
225 has been arid to semi-arid since at least the late Jurassic (Hartley et al., 2005), arid
226 since the late Oligocene and predominantly hyperarid since the mid Miocene
227 (Evenstar et al., 2009, Jordan et al., 2014, Evenstar et al., 2017, Rech et al., 2019).
228 Since the Oligocene, short intervals (< 1 myr) of slightly more humid conditions have
229 been recorded (Evenstar et al., 2009, 2015, 2017; Jordan et al., 2014) (Fig. 2). These
230 humid intervals are within the range of an arid climate with annual mean precipitation
231 rates less than 100 mm/yr, below the threshold for the establishment of significant
232 vegetation cover (Jordan et al., 2014). As a result of the long-lived regional persistent
233 climatic aridity, the PPS is exceptionally well preserved, providing a unique
234 opportunity to examine the development of regionally extensive paleo-fluvial surfaces
235 in a non-vegetated regime over geologic time-scales.

236

237 **4. Methodology and Approach**

238

239 **4.1 Reconstructing regional fluvial palaeo-surfaces.**

240

241 Relict paleo-surfaces of the PPS combined with the elevation data in the Longitudinal
242 Valley were used to identify and extrapolate geomorphic surfaces (pediments and
243 valley bottoms) throughout the past ca. 11 Myr. Four regional elevation profiles (A-D)
244 were constructed across the PPS, one parallel to the drainage (A-East to West) and
245 three perpendicular to the drainage (B, C and D-North to south) (Fig. 3). The
246 landscape profiles were constructed using DEM data from Shuttle Radar Topography
247 Mission (SRTM) data with 30 m resolution (Figs. 3 and 4). Profile A is 45 km long and
248 runs from east to west at 18°45'S (Fig. 3). The three other topographic profiles are
249 260 km long and run parallel along the eastern edge of the Longitudinal Valley from
250 southern Peru at 18°05'S towards northern Chile at 20°15'S (Location in Figure 3
251 and cross sections in Figure 4). These profiles cross three of the main paleo-
252 surfaces mapped within the regions (AS4, DS3 and DS2) (Fig. 3). On each profile the
253 remnant parts of the various paleo-surfaces (as mapped by Evenstar et al, 2017) are
254 highlighted (Figs.3 and 4). Using the preserved remnants of these surfaces
255 (palaeosurface residual highs, inset terraces and valley bottom elevations) we can
256 extrapolate the line of maximum incision levels of the main quebradas across the
257 region (Figs.3 and 4).

258

259

260 Surface AS4 is formed as a series of relict distributive fluvial systems with a low
261 gradient slope and is preserved on the west edge of profile A forming a plateau (Fig.
262 3). Using the slope of AS4, the surface can be projected towards the east (Fig. 3).
263 Within profiles B-D, AS4 is preserved in the south as a series of relict inselberg
264 surfaces which can be correlated across the southern region to reconstruct the paleo
265 fluvial surface (Fig. 4). Towards the north of Quebrada Camarones, the preservation
266 of the AS4 surface decreases and the surface cannot be accurately mapped north of
267 Quebrada Lluta.

268

269 Surface DS3 formed as a tributive fluvial system incised into AS4. It is well preserved
270 within the central parts of profile A cutting into AS4 and forming a low angle erosional
271 surface. This surface can be projected to the east using the slope angle (Fig. 3).
272 Within profiles B-D, DS3 is mapped as a series of relict inselberg highs north of
273 Quebrada Lluta (Figs. 4 and 5A-B). These highs in profiles B-D can be linked across
274 the region forming a single surface down to Quebrada Camarones. South of this
275 point, where AS4 is preserved, DS3 incises into AS4 and forms a series of lower
276 terraces (Figs. 4 and 5C).

277

278 Surface DS2 is preserved along the eastern edge of Profile A cutting into DS3 and
279 forming a low angle erosional surface (Fig. 3). Within Profiles B to D, this surface
280 forms the lowest incision surface north of Quebrada Lluta that can be correlated
281 across this region (Figs. 4 and 5A-B). Towards the south, this surface is constrained
282 within the main quebradas and forms a series of terraces. The Lluta ignimbrite is
283 preserved along these terraces and has previously been used to reconstruct the relict
284 river profiles at 2.7 Ma along the Quebrada Lluta which can be linked with this
285 surface (Kober et al. 2006).

286

287 In the southernmost part of the region the laterally traced fluvial archives are
288 correlated with the depths and timing of water table drops in the Cerro Colorado mine
289 that have been reconstructed using hematite age-dates from drill core (Cooper et al.
290 2016) (Fig. 4). Throughout the region, the present-day fluvial cross-profiles were
291 reconstructed utilising the lowermost incisional points within the modern-day
292 perennial rivers (Fig. 4).

293

294 **4.2 Palaeo-surface age constraints.**

295

296 Age constraints on the surfaces are based on previously published *insitu* exposure
297 age dating (Kober et al., 2007, Evenstar et al., 2009, Evenstar et al., 2017), dated
298 volcanics (Wörner et al., 2002, Kober et al., 2006, Hoke et al., 2007) and hematite
299 age-dates from drill core (Cooper et al., 2016). These constraints are shown where
300 they intersect the elevation profiles in Figure 4.

301

302 Surface AS4 is constrained as having formed between ~16-8 Ma (Hoke et al., 2007,
303 Evenstar et al., 2015). Within Quebrada Aroma (Fig. 1), the Nama ignimbrite is
304 interbedded with sediments that underlie surface AS4 placing an upper age
305 constraint of 16.27 ± 0.16 Ma on this surface (Pinto et al., 2004, Victor et al., 2004;
306 Farías et al., 2005; Pinto et al., 2007). Proximal to Quebrada Tana (Figs.1 and 4), the
307 Tana lava overlying this surface is dated at 8.8 ± 0.5 Ma (Mortimer et al., 1974 and
308 8.2 ± 0.5 Ma; Muñoz and Sepulveda, 1992) placing an upper age constraint on the
309 surface (Hoke et al., 2007). This surface is further constrained by *insitu* exposure
310 age dating to ~11 Ma (Fig. 4) (Evenstar et al., 2009, Evenstar et al., 2015 and
311 Evenstar et al., 2017).

312

313 Surface DS3 is constrained using *insitu* exposure age dating across the region to ~7
314 Ma (Kober et al., 2006, Evenstar et al., 2009, 2017). Several of the *insitu* exposure
315 ages lie on the landscape cross-profiles either on top of the residual palaeosurfaces
316 in the north or on the incised terrace surfaces in the south and are highlighted in
317 Figures 4 and 5C. Proximal to the Cerro Colorado mine DS3 links with the depth and
318 age of dated hematite within drill core at 7 Ma which records the paleowater table
319 level (Cooper et al., 2016) (Figure 4).

320

321 Surface DS2 was dated at ~3 Ma based on *insitu* exposure age dating (Fig. 4)
322 (Kober et al., 2006, Evenstar et al., 2009, 2017). The surface age can be further
323 constrained using the preservation of the Lluta ignimbrite (dated at 2.7 Ma; Wörner et
324 al., 2002) along fluvial terraces within Quebradas Lluta and Azapa (Fig. 4). Proximal
325 to the Cerro Colorado mine this surface is linked to dated hematite (3 Ma) within drill
326 core (Cooper et al., 2016) (Fig. 4).

327

328 **4.3 Reconstructing regional mean incision rates.**

329

330 The reconstructed fluvial paleo-surface profiles combined with the dating constraints
331 described above can be used to calculate the regional fluvial incision rates over the
332 last 11 million years (Fig. 6A). The difference in elevation between the paleo-fluvial

333 surfaces and modern river were extrapolated for each surface across the region (Fig.
334 6B). Using the difference in elevation of the surfaces and the modern river, divided by
335 the time since the surfaces had been abandoned the mean fluvial incision rates along
336 the main quebradas were calculated (Fig. 6C). In this way, we are able to reconstruct
337 relative incision rates for the PSS.

338

339 **5. Results**

340

341 Profile A runs 45 km from east to west at 18°45'S in Figure 3 and highlights the
342 general relationship of the surfaces within the region. AS4 is predominantly
343 preserved in the west of the Longitudinal Valley and shows an average depositional
344 slope of 5° to the west. Cutting into AS4 within the centre of the Longitudinal Valley,
345 DS3 incises 90 m and shows a similar depositional slope angle. To the east of DS3,
346 DS2 cuts 90 m into and erodes DS3, with a higher slope angle of 10° to the
347 west. Figure 4 highlights the overall relationship of the main fluvial archives from
348 North to South. AS4 forms the highest elevation surface across the region and is
349 predominantly preserved in the southern parts of the elevation profiles. DS3 cuts into
350 AS4 forming a lower elevation surface across the region. Cutting into both AS4 and
351 DS3, DS2 forms at the lowest elevation of all the preserved paleo-fluvial surface in
352 the Longitudinal Valley. The modern river system forms at the base of the valleys
353 with the lowermost elevations across the region. All the surfaces generally show an
354 increase in elevation towards the east and south across the region (Figure 3 and 4).
355 The changes in elevation show a step like increase from north to south and can be
356 separated into three different sectors (1 to 3 on Figure 4). Sector 1 runs from
357 (18°05'S) to Quebrada Tana (19°20'S), Sector 2 from Quebrada Tana (19°20'S) to
358 Quebrada Tarapaca (19°50'S) and Sector 3 from Quebrada Tarapaca (19°50'S) to
359 Quebrada Juan de Morales (20°10'S). Within each sector the change in elevation is
360 broadly similar and affects a number of different rivers rather than being river
361 specific. Sector 1 shows the highest changes in elevation across the region between
362 the different fluvial surfaces which decrease within Sector 2 and is the lowest within
363 Sector 3.

364

365 Figure 6A shows the current elevation of the fluvial systems in cross section B. AS4
366 shows a single laterally extensive surface which undulates across the region from
367 ~2750 masl in Sector 1, to ~2500 masl in Sector 2 and ~2650 masl in Sector 3. DS3
368 forms a laterally extensive surface with an average height of 2350 masl across
369 Sector 1 and 2 and increasing in elevation to ~2700 masl in Sector 3. DS2 varies in

370 elevation from 1800 masl at the northern tip of the elevation profile to ~ 2000 masl in
371 Sector 2 and increases in height to ~2600 masl in Sector 3. The modern fluvial
372 systems vary in height from 1400 masl to 1500 masl in Sector 1 to Sector 2 to ~2000
373 masl and ~2500 masl in Sector 3.

374

375 Using the difference between the paleo fluvial surfaces and modern fluvial systems
376 the change in fluvial incision through time can be more clearly illustrated (Fig. 6B).
377 and combined with the age constraint the fluvial incision rates through time can be
378 calculated (Fig. 6C). Overall, fluvial incision shows higher rates from 3 to present
379 day. However, there are marked differences across the study area. Sector 1 show
380 the highest rates of fluvial incision through time from 120 m/Myr at 11-7 Ma to 150
381 m/Myr at 7-3 Ma to ~200 m/Myr at 3-0 Ma. Sector 2 show lower incision rates
382 through time of 50 m/My for both 11-7 Ma and 7-3 Ma and higher rates of 100-50 for
383 3-0 Ma. Sector 3 show the lowest rates of fluvial incision throughout the area with 25
384 m/Myr from 11-7 Ma, 30m/Myr from 7-3 Ma and 50 m/Myr from 3-0 Ma.

385

386 **6. Discussion**

387

388 The geomorphic archive, using both pediplain and fluvial surfaces, is reconstructed
389 from Northernmost Chile and combined with age constraints to calculate fluvial
390 incision rates over a continental scale (>250 km) and back to the Miocene. These
391 data demonstrate three spatially marked changes in incision rates across the region,
392 from north to south. These distinctly different regions have been termed Sectors 1-3.
393 Sector 1 has the highest rates of fluvial incision through time (ca. 200 to 100 m/Myr),
394 Sector 2 show a lower rate of incision (ca. 100 to 50 m/Myr) and Sector 3 has the
395 lowest rates of incision (<50 m/Myr). These profiles show a generally continuous
396 drop in fluvial incision with slightly higher incision from 3 Ma to the present day. This
397 study shows that along the western margin of the Andes rates of fluvial incision can
398 vary dramatically over distances of 10's to 100's km. In Sector 1, incision rates of 100
399 m/m.y support those proposed by Hoke et al., (2007). However, in contrast to Hoke
400 et al., (2007) the incision shows a marked decrease to the south of Section 1 with
401 substantially lower rates in Section 2 and Section 3. These low rates correlate with
402 the incision rates documented in Cooper et al., (2016) explaining the disparity
403 between these two studies. Below we discuss what controls the variation in incision
404 rates in this region in order to evaluate their use as surface uplift makers.

405

406 The spatial extent of the area impacted (i.e. affecting multiple rivers per area

407 simultaneously) implies an external control. Such a control could take the form of (but
408 is not limited to) a change in relative terminal base level, climate or regional scale
409 tectonic uplift through fault blocks, rather than more localised internal river/catchment
410 specific causes (e.g. internal drainage reorganisation via river capture). Below we
411 discuss the major external controls on the compartmentalisation of the rivers within
412 this region.

413

414 **6.1 Uplift and fluvial incision**

415

416 **Regional tectonic uplift**

417 Fluvial incision rates have been used in numerous studies to help constrain uplift in
418 tectonically active areas (Maddy et al. 1997; Lave and Avouac 2001; Lu et al. 2004;
419 Whittaker et al., 2007). Although fluvial incision rates do not necessarily directly
420 translate to uplift rates as discharge may limit erosional capacity, they do give
421 minimum constraints. The sustained regional uplift of the Andean mountain chain is
422 broadly mirrored by continuous tectonically-driven fluvial incision throughout the
423 Miocene. However, this uplift is predominantly controlled by north-south fault
424 systems creating variation in uplift from West to East. There are no large scale east-
425 west trending structures which would generate marked changes in regional tectonic
426 uplift from North to South accounting for the compartmentalisation of the fluvial
427 incision rates.

428

429 **Terminal base level**

430 Comparison of Sector 1 and Sector 2 suggests a marked decrease in fluvial incision
431 through time and a marked change in terminal base level between the two fluvial
432 regions. In this part of the Andes the terminal base level is either external (sea level)
433 north of Quebrada Tana or internal (the Longitudinal valley, 1000 masl) south of
434 Quebrada Tana. Uniquely, Quebrada Tana acts as an endorheic drainage within the
435 Longitudinal Valley (Garcia et al., 2011; Kirk-Lawlor et al., 2013; Evenstar et al.,
436 2017). The timing of when fluvial systems north of Quebrada Tana became
437 exorheicly drained is diachronous from the Early to Mid Miocene *prior* to the fluvial
438 incision documented here (Evenstar et al., 2017). A change in base level would
439 initially lead to river profile adjustment affecting individual drainages, the absence of
440 observable river specific differences in the fluvial archives support the idea that in
441 Sector 1 rivers had an exorheic drainage prior to 11 Ma and so do not explain the
442 difference in fluvial incision rates between Sector 1 and Sector 2. However, the uplift
443 of the Coastal Cordillera has not been static during this time period. The uplift rate of

444 the Coastal Cordillera is poorly constrained, as discussed above. The base level of
445 the fluvial systems in the Longitudinal Valley terminate onto the eastern edge of the
446 Coastal Cordillera and are therefore affected by the regional scale uplift of the
447 mountain range rather than the uplift proximal to the coast which may be more
448 variable. The large scale and long term uplift of the mountain range varies from
449 between 50 m/Myr (0.05 mm/yr) to 70 m/Myr (0.07 mm/yr) (Delouis et al. 1998;
450 Hartley et al. 2000; Dunai et al. 2005; Cosentino and Jordan 2017). The difference
451 between the fluvial incision rate at Sector 1 compared to Sector 2, averaged over 11
452 Ma is 60m/Myr correlating with this value. Consequently, whilst Andean uplift to the
453 east generated significant fluvial incision within the Longitudinal Valley this was
454 partially offset in Sector 2 and 3 (the endorheicly-drained region) by simultaneous
455 uplift of the Coastal Cordillera in the west. In essence, the rate of fluvial incision is
456 controlled by the east to west length of the fluvial system and whether rivers cut the
457 uplifting north-south trending Coastal Cordillera. The difference between the reach of
458 Sector 1 and Sector 2 is highlighted in Figure 1B.

459

460 **Tectonic beheading**

461

462 The change in fluvial incision rates from Sector 2 to 3 are more challenging to
463 explain. Both sectors have the same terminal base level within the Longitudinal
464 Valley of ~1000 masl. However, there is a sharp change in the catchment length of
465 major fluvial systems entering the Longitudinal Valley from between the two regions
466 (Fig. 7). Throughout the region, 18°20'S to 22°00' S, the fluvial systems have been
467 constrained by Hoke et al., 2007 as ranging in drainage area from 5×10^9 km² to $9 \times$
468 10^8 km² and in length from 30 to 170 km, with both values decreasing towards the
469 south (Fig. 7). Significantly, these data demonstrate a sudden decrease in fluvial
470 lengths from 110 km to 80 km between Sector 2 and Sector 3 (Figs. 1 and 7). This
471 length-gap coincides with a sudden shift in the edge of the watershed from along the
472 western edge of the Western Cordillera to along the Cordillera de Domeyko fault
473 system in the central Precordillera suggesting a tectonically configured watershed.
474 The uplift along the Cordillera de Domeyko fault system beheads the upper part of
475 the drainages within Sector 3, reducing their length by approx. 30 km (Figs. 1 and 7).
476 The affected fluvial systems in this region thus only record the minimum uplift over
477 the Longitudinal Valley and Precordillera as they are no longer connected to the
478 highest elevation areas of the mountain range further east (Fig. 1B). The difference
479 in fluvial incision rates between Sector 2 and Sector 3 of 25 m/Myr to 50 m/Myr
480 therefore place constraints on the uplift generated between the central and eastern

481 edge of the Precordillera.

482

483 **6.2 Alternative controls on fluvial incision**

484

485 Whilst the observed spatial differences in fluvial incision rates over the region can be
486 largely explained by tectonic controls it is important to briefly explore alternative
487 explanations for these regional differences within the study area that can operate on
488 a similar spatial scale, principally climate and bedrock. It has been suggested that the
489 present-day rivers within the study area vary in erosional capacity from north to south
490 as a function of mean annual precipitation within the source regions (Garcia et al
491 2011). Quebrada Lluta has a catchment with a present-day mean annual
492 precipitation rate of 200 mm/yr, Quebradas Azapa, Victor and Camarones have rates
493 of 100 mm/yr and south of Quebrada Camarones the river catchments have rates of
494 < 100 mm/yr (Garcia et al., 2011). However, it is unlikely that latitudinal variations in
495 rainfall are the main cause for incision patterns observed across the region as there
496 is no apparent spatial link between the precipitation rates and the change in fluvial
497 incision rates. For example, there is no change in the fluvial incision between
498 Quebrada Lluta and the rivers to the south, despite Quebrada Lluta draining an area
499 with much higher mean annual precipitation. If precipitation rates do place some
500 control on incision rates it must be at a much smaller scale than the tectonic controls.

501

502 Fluvial research demonstrates that the strength properties of bedrock lithology can
503 impact on fluvial system incisional behaviour (e.g. Stokes et al., 2017) and could thus
504 potentially account for spatial variations in incision rates across the study area.

505 However, whilst there is a difference *between* the major N-S morphotectonic units
506 (thereby presenting an E-W variability in potential erodibility across the region), there
507 is little N-S variation *within* these units that can account for the observed N-S
508 spatially compartmentalised incision rates.

509

510 **6.3 Controls on fluvial incision in Northern Chile**

511

512 Fluvial incision rates have been used in numerous studies to help constrain uplift in
513 tectonically active areas (Lave and Avouac 2001; Lu et al. 2004; Whittaker et al.,
514 2007; Anton et al., 2014; Stokes et al. 2018). The fluvial regions along the edge of
515 the Andes have varying east-west extent over the north-south orientated tectonic
516 provinces. The fluvial incision therefore shows marked compartmentalization across
517 the region with a step like increase from south to north. The varying reaches of the

518 rivers and the differences in fluvial incision rates between these reaches can
519 therefore be exploited to place minimum constraints on the different tectonic
520 provinces through time.

521

522 Sector 1, which spans from the Pacific Ocean to the western edge of the Western
523 Cordillera (Figure 1B), constrains the uplift on a continental-scale along the edge of
524 the Andes. This constrains the uplift of this region (the western side of the Andes) to
525 a minimum of 1200m in 11 Myr. This supports previous models of Late Miocene uplift
526 (e.g. Garzzone et al., 2006; Ghosh et al., 2006, Garzzone et al., 2008) however in
527 contrast to these models it suggests uplift continued at a slower rate from 7 to 3 Ma
528 and at a higher rates from 3 to 0 Ma (120 m/Myr at 11-7 Ma to 150 m/Myr at 7-3 Ma
529 to ~200 m/Myr at 3-0 Ma).

530

531 Sector 2 spans from the Longitudinal Valley to the western edge of the Western
532 Cordillera (Fig. 1B) constraining the uplift over the western margin of the Andes
533 minus uplift of the Coastal Cordillera. Therefore, the difference between Sector 1 and
534 Sector 2 of 60 m/Myr records the uplift of the Coastal Cordillera which corresponds
535 with published uplift rates for the Coastal Cordillera of between 50 m/Myr (0.05
536 mm/yr) to 70 m/Myr (0.07 mm/yr) (Delouis et al. 1998; Hartley et al. 2000; Dunai et
537 al. 2005).

538

539 Sector 3, spans a much shorter extent than Sectors 1 and 2, from the Longitudinal
540 Valley to the Cordillera de Domeyko fault system in the central Precordillera (Fig.
541 1B). The difference between Sectors 2 and 3, of 25 m/Myr to 50 m/Myr, therefore
542 places a minimum constraint on the uplift generated between the central and eastern
543 edge of the Precordillera along the Cordillera de Domeyko fault system.

544

545 **7. Conclusions**

546

547 Within the Atacama Desert, Northern Chile, slow long-term erosion creates
548 exceptional preservation of geomorphic archives (fluvial and pediment surfaces)
549 allowing the long-term reconstruction of fluvial archives on a continental scale. In this
550 study, fluvial profiles are constructed over a wide region (>250 km) along the western
551 margin of the Andes (18°00'S to 20°15'S) and over a time frame from Miocene to
552 Present day. The results reveal that incision patterns reconstructed over a wide area
553 running perpendicular to the main fluvial systems allows a greater spatial and
554 temporal understanding of uplift, specifically;

555

556

- Fluvial incision can be reconstructed for ~11 Ma, ~7 Ma, ~3 Ma and the modern day.

557

558

- Fluvial incision shows marked spatial compartmentalization across the region with a step like increase from south to north.

559

560

- Sector 1 has the highest rates of fluvial incision through time (ca. 200 to 100 m/Myr), Sector 2 shows a lower rate of incision (ca. 100 to 50 m/Myr) and Sector 3 has the lowest rates of incision (<50 m/Myr).

561

562

563

- The main control on the rate of fluvial incision is the extent of the east to west reach of the main rivers across the north to south tectonic provinces.

564

565

- Sector 1 spans the entire Coastal Cordillera, Longitudinal Valley and Precordillera to the western edge of the Western Cordillera. This constrains uplift of this region (the western side of the Andes) to a minimum of 1200m in 11 Myr which supports Late Miocene uplift however contrary to these models, it suggests uplift continued at a higher rate from 3 to the present day.

566

567

568

569

570

- Sector 2 only spans the Longitudinal Valley and the Precordillera to the western edge of the Western Cordillera. The absence of fluvial systems cutting the Coastal Cordillera accounts for the reduced incision rates of 60 m/Myr which correspond to the published uplift rates for the Coastal Cordillera of 60 m/Myr.

571

572

573

574

575

- The eastern edge of Sector 3 is constrained by the Cordillera Domeyko fault system within the Central Precordillera. As such, Sector 3 only places constraints on uplift of the Longitudinal Valley and the western edge of the Precordillera. The absence of the eastern edge of the Precordillera accounts for the decrease in incision rates within this area and places a constraint of uplift generated here in the region of 25 m/Myr to 50 m/Myr.

576

577

578

579

580

581

582

Most Quaternary fluvial studies tend to be restricted to detailed examination of a single river to understand long-term uplift or climate, mainly due to the scale and intensity of research required to unravel the incision history. Whilst this provides a wealth of knowledge regarding uplift over the reach of the fluvial system, in order to understand orographic scale uplift (and rule out river specific controls) a more regional overview of the fluvial base-level changes is required. Such studies have the potential to address not just the timing of uplift on a continental scale but also any regional spatial controls such as the relative uplift of individual tectonic provinces.

583

584

585

586

587

588

589

590

591 **8. Acknowledgements**

592

593 This study was funded by BHP and the University of Brighton Rising Stars. The
594 authors are grateful to Marit Van Zalinge and Masie Mather for discussions on the
595 manuscript.

596

597 **9. References**

598

599 Antón, L., De Vicente, G., Muñoz-Martín, A., & Stokes, M. (2014). Using river long
600 profiles and geomorphic indices to evaluate the geomorphological signature of
601 continental scale drainage capture, Duero basin (NW Iberia). *Geomorphology*, 206,
602 250-261.

603

604 Barnes, J. B., & Ehlers, T. A. (2009). End member models for Andean Plateau uplift.
605 *Earth-Science Reviews*, 97(1-4), 105-132.

606

607 Benito, G., Gutiérrez, F., Pérez-González, A., & Machado, M. J. (2000).
608 Geomorphological and sedimentological features in Quaternary fluvial systems
609 affected by solution-induced subsidence (Ebro Basin, NE-
610 Spain). *Geomorphology*, 33(3-4), 209-224.

611

612 Boulton, S. J., Stokes, M., & Mather, A. E. (2014). Transient fluvial incision as an
613 indicator of active faulting and Plio-Quaternary uplift of the Moroccan High
614 Atlas. *Tectonophysics*, 633, 16-33.

615

616 Bridgland, D. R., Westaway, R., Romieh, M. A., Candy, I., Daoud, M., Demir, T. &
617 Shaw, A. D. (2012). The River Orontes in Syria and Turkey: Downstream variation of
618 fluvial archives in different crustal blocks. *Geomorphology*, 165, 25-49.

619

620 Cooper, F., Adams, B., Blundy, J., Farley, K., McKeon, R., & Ruggiero, A. (2016).
621 Aridity-induced Miocene canyon incision in the Central Andes. *Geology*, 44(8), 675-
622 678.

623

624 Cosentino, N. J., Jordan, T. E., Derry, L. A., & Morgan, J. P. (2015). $^{87}\text{Sr}/^{86}\text{Sr}$ in
625 recent accumulations of calcium sulfate on landscapes of hyperarid settings: A
626 bimodal altitudinal dependence for northern Chile (19.5°S – 21.5°S). *Geochemistry,*
627 *Geophysics, Geosystems*, 16(12), 4311-4328.

628

629

630 Cyr, A. J., Granger, D. E., Olivetti, V., & Molin, P. (2010). Quantifying rock uplift rates
631 using channel steepness and cosmogenic nuclide-determined erosion rates:
632 Examples from northern and southern Italy. *Lithosphere*, 2(3), 188-198.

633

634 Delouis, B., Philip, H., Dorbath, L., & Cisternas, A. (1998). Recent crustal
635 deformation in the Antofagasta region (northern Chile) and the subduction process.
636 *Geophysical Journal International*, 132(2), 302-338.

637

638 Demoulin, A., Bovy, B., Rixhon, G., & Cornet, Y. (2007). An automated method to
639 extract fluvial terraces from digital elevation models: The Vesdre valley, a case study
640 in eastern Belgium. *Geomorphology*, 91(1-2), 51-64.

641

642 Demoulin, A., Mather, A., & Whittaker, A. (2017). Fluvial archives, a valuable record
643 of vertical crustal deformation. *Quaternary Science Reviews*, 166, 10-37.

644

645 Dunai, T. J., Gonzalez-Lopez, G. A., Juez-Larre, J., & Carrizo, D. (2005).
646 Preservation of (early) miocene landscapes in the Atacama Desert, northern Chile.
647 *Geochimica Et Cosmochimica Acta*, 69(10), A161-A161.

648

649 Ehlers, T. A., & Poulsen, C. J. (2009). Influence of Andean uplift on climate and
650 paleoaltimetry estimates. *Earth and Planetary Science Letters*, 281(3-4), 238-248.

651

652 Evenstar, L., Mather, A., Hartley, A., Stuart, F., Sparks, R., & Cooper, F. (2017).
653 Geomorphology on geologic timescales: Evolution of the late Cenozoic Pacific
654 paleosurface in Northern Chile and Southern Peru. *Earth-Science Reviews*. 71, 1-27.

655

656 Evenstar, L. A., Hartley, A. J., Stuart, F. M., Mather, A. E., Rice, C. M., & Chong, G.
657 (2009). Multiphase development of the Atacama Planation Surface recorded by
658 cosmogenic He-3 exposure ages: Implications for uplift and Cenozoic climate change
659 in western South America. *Geology*, 37(7), 658-658.

660

661 Evenstar, L. A., Stuart, F. M., Hartley, A. J., & Tattitch, B. (2015). Slow Cenozoic
662 uplift of the western Andean Cordillera indicated by cosmogenic ³He in alluvial
663 boulders from the Pacific Planation Surface. *Geophysical Research Letters*, 42(20),
664 8448-8455.

665

666 Evenstar, L. A., Sparks, R. S. J., Cooper, F. J., & Lawton, M. N. (2018). Quaternary
667 landscape evolution of the Helmand Basin, Afghanistan: Insights from staircase
668 terraces, deltas, and paleoshorelines using high-resolution remote sensing
669 analysis. *Geomorphology*, 311, 37-50.

670

671 Farías, M., Charrier, R., Comte, D., Martinod, J., & Hérail, G. (2005). Late Cenozoic
672 deformation and uplift of the western flank of the Altiplano: Evidence from the
673 depositional, tectonic, and geomorphologic evolution and shallow seismic activity
674 (northern Chile at 19°30'S). *Tectonics*, 24(4), TC4001.

675

676 Garcia, M., & Herail, G. (2005). Fault-related folding, drainage network evolution and
677 valley incision during the Neogene in the Andean Precordillera of Northern Chile.
678 *Geomorphology*, 65(3-4), 279-300.

679

680 Garcia, M., Riquelme, R., Farías, M., Herail, G., & Charrier, R. (2011). Late Miocene-
681 Holocene canyon incision in the western Altiplano, northern Chile: tectonic or climatic
682 forcing? *Journal of the Geological Society*, 168(4), 1047-1060.

683

684 García-Pérez, T., Marquardt, C., Yáñez, G., Cembrano, J., Gomila, R., Santibañez,
685 I., & Maringue, J. (2018). Insights on the structural control of a Neogene forearc
686 basin in Northern Chile: A geophysical approach. *Tectonophysics*, 736, 1-14.

687

688 Garzione, C. N., Hoke, G. D., Libarkin, J. C., Withers, S., MacFadden, B., Eiler, J. &
689 Mulch, A. (2008). Rise of the Andes. *Science*, 320(5881), 1304-1307.

690

691 Garzione, C. N., Molnar, P., Libarkin, J. C., & MacFadden, B. J. (2006). Rapid late
692 Miocene rise of the Bolivian Altiplano: Evidence for removal of mantle lithosphere.
693 *Earth and Planetary Science Letters*, 241(3-4), 543-556.

694

695 Gesch, D. B. (2014). An inventory of topographic surface changes; the value of
696 multitemporal elevation data for change analysis and monitoring. *ISPRS Annals of*
697 *Photogrammetry, Remote Sensing & Spatial Information Sciences*, 2(4).

698

699 Ghosh, P., Garzione, C. N., & Eiler, J. M. (2006). Rapid uplift of the Altiplano
700 revealed through C-13-O-18 bonds in paleosol carbonates. *Science*, 311(5760), 511-
701 515.

702

703 Hartley, A. J., Chong, G., Houston, J., & Mather, A. E. (2005). 150 million years of
704 climatic stability: evidence from the Atacama Desert, northern Chile. *Journal of the*
705 *Geological Society*, 162(3), 421-424.

706

707 Hartley, A. J., & Evenstar, L. (2010). Cenozoic stratigraphic development in the north
708 Chilean forearc: Implications for basin development and uplift history of the Central
709 Andean margin. *Tectonophysics*, 495(1-2), 67-77.

710

711 Hartley, A. J., May, G., Chong, G., Turner, P., Kape, S. J., & Jolley, E. J. (2000).
712 Development of a continental forearc: A Cenozoic example from the Central Andes,
713 northern Chile. *Geology*, 28(4), 331-334.

714

715 Hartley, A. J., Sempere, T., & Wörner, G. (2007). A comment on "Rapid late Miocene
716 rise of the Bolivian Altiplano: Evidence for removal of mantle lithosphere" by C.N.
717 Garzione et al. [*Earth Planet. Sci. Lett.* 241 (2006) 543-556]. *Earth and Planetary*
718 *Science Letters*, 259(3-4), 625-629.

719

720 Hoke, G. D., Isacks, B. L., Jordan, T. E., Blanco, N., Tomlinson, A. J., & Ramezani, J.
721 (2007). Geomorphic evidence for post-10 Ma uplift of the western flank of the central
722 Andes 18°30'-22°S. *Tectonics*, 26(5), TC5021

723

724

725 Hu, X., Pan, B., Kirby, E., Li, Q., Geng, H., & Chen, J. (2010). Spatial differences in
726 rock uplift rates inferred from channel steepness indices along the northern flank of
727 the Qilian Mountain, northeast Tibetan Plateau. *Chinese Science Bulletin*, 55(27-28),
728 3205-3214.

729

730 Jordan, T. E., Kirk-Lawlor, N. E., Blanco P., N., Rech, J. A., & Cosentino, N. J.
731 (2014). Landscape modification in response to repeated onset of hyperarid
732 paleoclimate states since 14 Ma, Atacama Desert, Chile. *Geological Society of*
733 *America Bulletin*. 126(7/7), 1016-1046

734

735 Juez-Larré, J., Kukowski, N., Dunai, T. J., Hartley, A. J., & Andriessen, P. A. (2010).
736 Thermal and exhumation history of the Coastal Cordillera arc of northern Chile
737 revealed by thermochronological dating. *Tectonophysics*, 495(1), 48-66.

738

739 Kirk-Lawlor, N. E., Jordan, T. E., Rech, J. A., & Lehmann, S. B. (2013). Late Miocene
740 to Early Pliocene paleohydrology and landscape evolution of Northern Chile, 19 to 20
741 S. *Palaeogeography, Palaeoclimatology, Palaeoecology*, 387, 76-90.
742

743 Kober, F., Ivy-Ochs, S., Schlunegger, F., Baur, H., Kubik, P. W., & Wieler, R. (2007).
744 Denudation rates and a topography-driven rainfall threshold in northern Chile:
745 Multiple cosmogenic nuclide data and sediment yield budgets. *Geomorphology*, 83(1-
746 2), 97-120.
747

748 Kober, F., Schlunegger, F., Zeilinger, G., & Schneider, H. (2006). Surface uplift and
749 climate change: The geomorphic evolution of the Western Escarpment of the Andes
750 of northern Chile between the Miocene and present. *Tectonics, Climate, and
751 Landscape Evolution*, 398, 75-86.
752

753 Lavé, J., & Avouac, J.-P. (2000). Active folding of fluvial terraces across the Siwaliks
754 Hills, Himalayas of central Nepal. *Journal of Geophysical Research: Solid Earth*,
755 105(B3), 5735-5770.
756

757 Litchfield, N., & Berryman, K. (2006). Relations between postglacial fluvial incision
758 rates and uplift rates in the North Island, New Zealand. *Journal of Geophysical
759 Research: Earth Surface*, 111(F2).
760

761 Lu, H., Wang, X., An, Z., Miao, X. D., Zhu, R. X., Ma, H. Z., & Wang, X. Y. (2004).
762 Geomorphologic evidence of phased uplift of the north eastern Qinghai-Tibet Plateau
763 since 14 million years ago. *Science in the China Series D Earth Science-English
764 edition*, 47, 822-833.
765

766 Macklin, M. G., Fuller, I. C., Lewin, J., Maas, G. S., Passmore, D. G., Rose, J., &
767 Rowan, J. S. (2002). Correlation of fluvial sequences in the Mediterranean basin over
768 the last 200 ka and their relationship to climate change. *Quaternary Science
769 Reviews*, 21(14-15), 1633-1641
770

771 Maddy, D. (1997). Uplift-driven valley incision and river terrace formation in southern
772 England. *Journal of Quaternary Science: Published for the Quaternary Research
773 Association*, 12(6), 539-545.
774

775 Madella, A., Delunel, R., Audin, L., & Schlunegger, F. (2016). Why is there no

776 Coastal Cordillera at the Arica Bend (Western Central Andes)? Basin Research.
777 Mortimer C., F. E. a. S. N. (1974). K-Ar ages from tertiary lavas of the northernmost
778 Chilean Andes. *Geologische Rundschau*, 63, 484 - 493.
779
780 Martins, A. A., Cabral, J., Cunha, P. P., Stokes, M., Borges, J., Caldeira, B., &
781 Martins, A. C. (2017). Tectonic and lithological controls on fluvial landscape
782 development in central-eastern Portugal: Insights from long profile tributary stream
783 analyses. *Geomorphology*, 276, 144-163.
784
785 Montgomery, D. R., & Brandon, M. T. (2002). Topographic controls on erosion rates
786 in tectonically active mountain ranges. *Earth and Planetary Science Letters*, 201(3-
787 4), 481-489.
788
789 Muñoz, N., Sepúlveda, p. (1992). Estructuras compressivas con vergencia al Oeste
790 en el borde oriental de la Depresión Central (19°15' lat. Sur). *Revista Geologica De*
791 *Chile*, 19, 214-247.
792
793 Noble, D. C., Sébrier, M., Megard, F., & McKee, E. H. (1985). Demonstration of two
794 pulses of Paleogene deformation in the Andes of Peru. *Earth and Planetary Science*
795 *Letters*, 73(2), 345-349.
796
797 Pinto, L., Hérail, G., Charrier, R. (2004). Syntectonic sedimentation associated with
798 Neogene structures in the Precordillera of Moquella Zone, Tarapacá (19°15'S,
799 northern Chile). *Revista Geologica De Chile*, 31, 19-44.
800
801 Pinto, L., Hérail, G., Fontan, F., & de Parseval, P. (2007). Neogene erosion and uplift
802 of the western edge of the Andean Plateau as determined by detrital heavy mineral
803 analysis. *Sedimentary Geology*, 195(3-4), 217-237.
804
805 Rech, J. A., Currie, B. S., Jordan, T. E., Riquelme, R., Lehmann, S. B., Kirk-Lawlor,
806 N. E., & Gooley, J. T. (2019). Massive middle Miocene gypsic paleosols in the
807 Atacama Desert and the formation of the Central Andean rain-shadow. *Earth and*
808 *Planetary Science Letters*, 506, 184-194.
809
810 Regard, V., Saillard, M., Martinod, J., Audin, L., Carretier, S., Pedoja, K., ... & Hérail,
811 G. (2010). Renewed uplift of the Central Andes Forearc revealed by coastal evolution
812 during the Quaternary. *Earth and Planetary Science Letters*, 297(1-2), 199-210.

813

814 Schildgen, T., Dethier, D. P., Bierman, P., & Caffee, M. (2002). ²⁶Al and ¹⁰Be dating
815 of late Pleistocene and Holocene fill terraces: a record of fluvial deposition and
816 incision, Colorado Front Range. *Earth Surface Processes and Landforms*, 27(7),
817 773-787.

818

819 Schildgen, T. F., Ehlers, T. A., Whipp, D. M., van Soest, M. C., Whipple, K. X., &
820 Hodges, K. V. (2009). Quantifying canyon incision and Andean Plateau surface uplift,
821 southwest Peru: A thermochronometer and numerical modeling approach. *Journal of*
822 *Geophysical Research*, 114(F4).

823

824 Stokes, M., Mather, A., Belfoul, M., Faik, F., Bouzid, S., Geach, M., & Thiel, C.
825 (2017). Controls on dryland mountain landscape development along the NW Saharan
826 desert margin: Insights from Quaternary river terrace sequences (Dadès River,
827 south-central High Atlas, Morocco). *Quaternary Science Reviews*, 166, 363-379.

828

829 Stokes, M., Mather, A., Rodés, Á., Kearsey, S., & Lewin, S. (2018). Anatomy, age
830 and origin of an intramontane top basin surface (Sorbas Basin, Betic Cordillera, SE
831 Spain). *Quaternary*, 1(2), 15

832

833 Thouret, J.-C., Wörner, G., Gunnell, Y., Singer, B., Zhang, X., & Souriot, T. (2007).
834 Geochronologic and stratigraphic constraints on canyon incision and Miocene uplift
835 of the Central Andes in Peru. *Earth and Planetary Science Letters*, 263(3), 151-166.

836

837 van Zalinge, M. E., Sparks, R. S. J., Evenstar, L. A., Cooper, F. J., Aslin, J., &
838 Condon, D. J. (2017). Using ignimbrites to quantify structural relief growth and
839 understand deformation processes: Implications for the development of the Western
840 Andean Slope, northernmost Chile. *Lithosphere*, 9(1), 29-45.

841

842 Victor, P., Oncken, O., & Glodny, J. (2004). Uplift of the western Altiplano plateau:
843 Evidence from the Precordillera between 20° and 21°S (northern Chile). *Tectonics*,
844 23(4), TC4004.

845

846 Wörner, G., Hammerschmidt, K., Henjes-Kunst, F., Lezaun, J., & Wilke, H. (2000).
847 Geochronology (⁴⁰Ar/³⁹Ar, K-Ar and He-exposure ages) of Cenozoic magmatic
848 rocks from northern Chile (18-22 S): implications for magmatism and tectonic
849 evolution of the central Andes. *Revista geológica de Chile*, 27(2), 205-240.

850

851 Whittaker, A. C., Cowie, P. A., Attal, M., Tucker, G. E., & Roberts, G. P. (2007).

852 Bedrock channel adjustment to tectonic forcing: Implications for predicting river

853 incision rates. *Geology*, 35(2), 103-106.

854

855 Wörner, G., Uhlig, D., Kohler, I., & Seyfried, H. (2002). Evolution of the West Andean

856 Escarpment at 18°S (N. Chile) during the last 25 Ma: uplift, erosion and collapse

857 through time. *Tectonophysics*, 345(1–4), 183-198.

858

859 Wotzlaw, J. F., Decou, A., von Eynatten, H., Wörner, G., & Frei, D. (2011). Jurassic

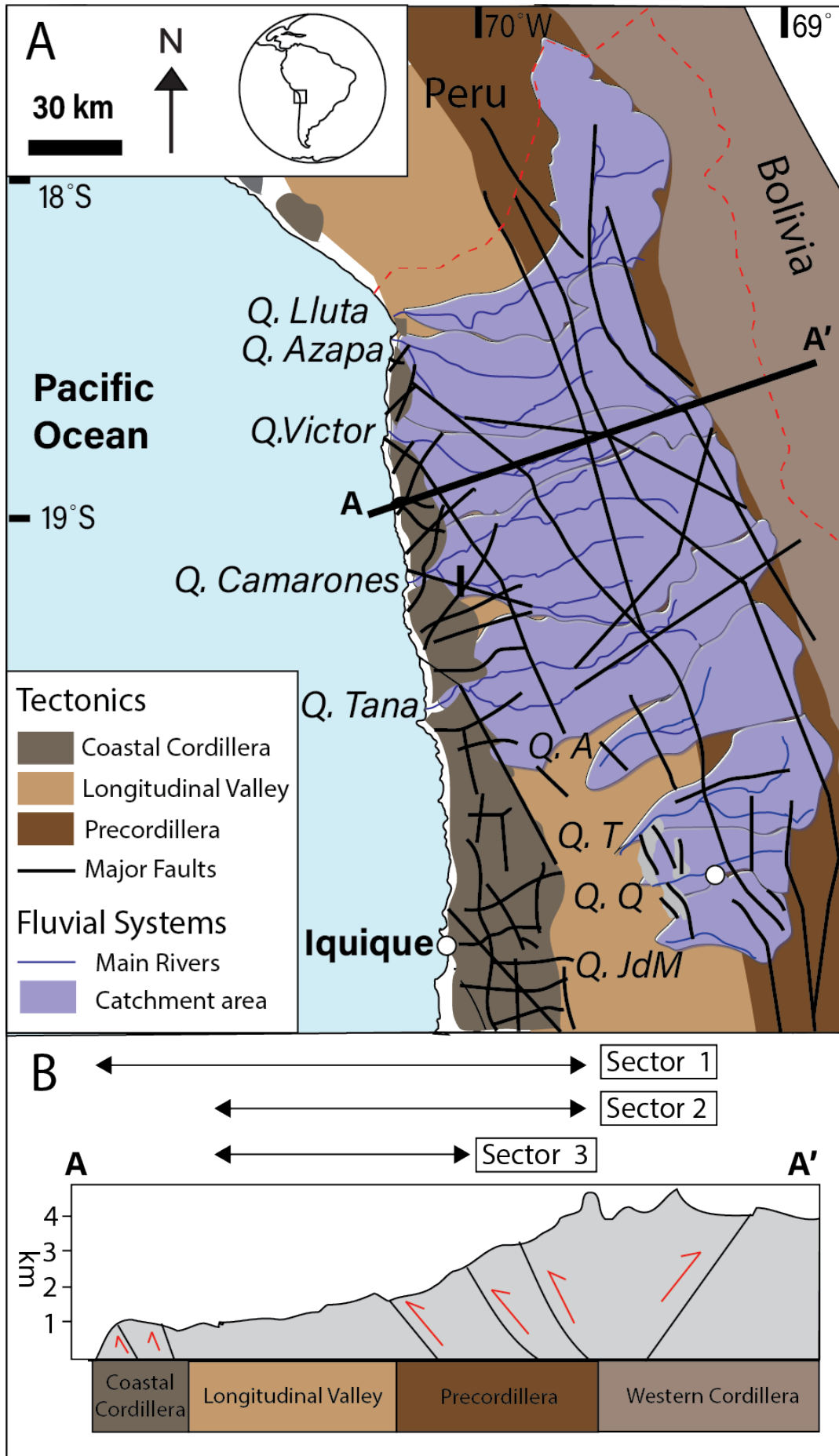
860 to Palaeogene tectono-magmatic evolution of northern Chile and adjacent Bolivia

861 from detrital zircon U-Pb geochronology and heavy mineral provenance. *Terra Nova*,

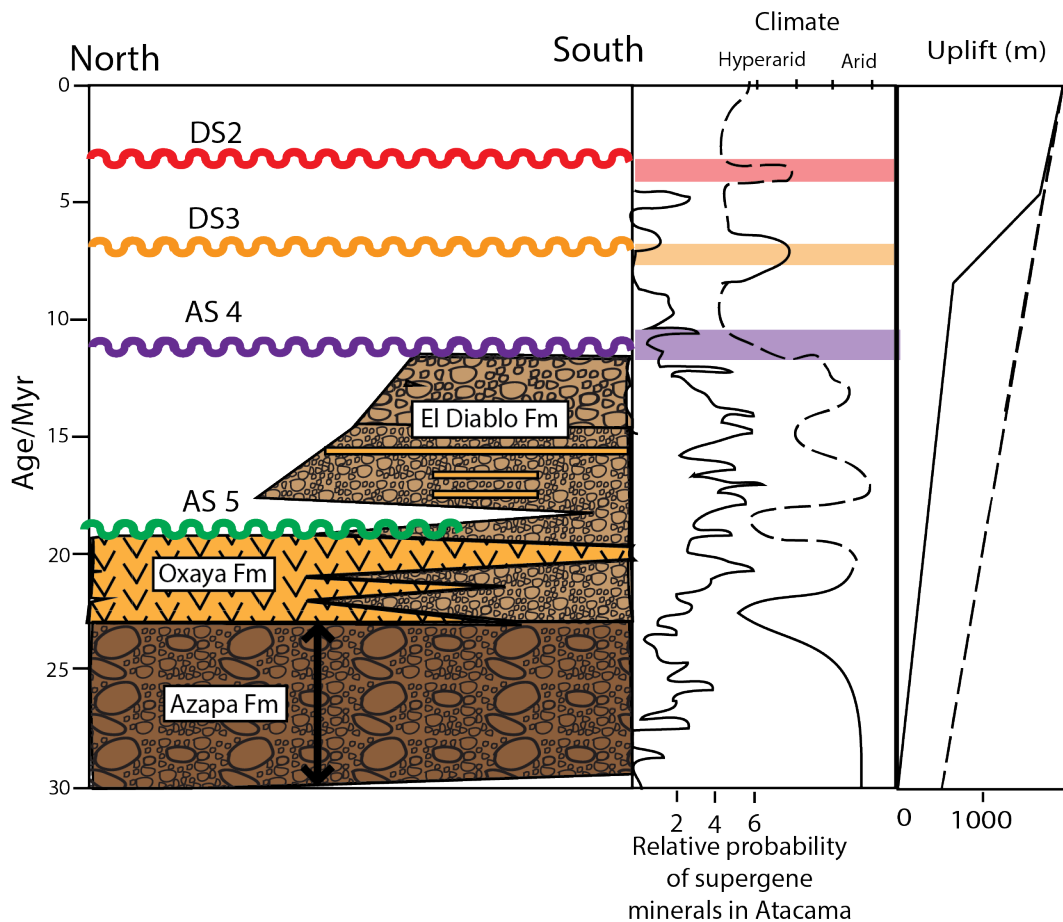
862 23(6), 399-406.

863

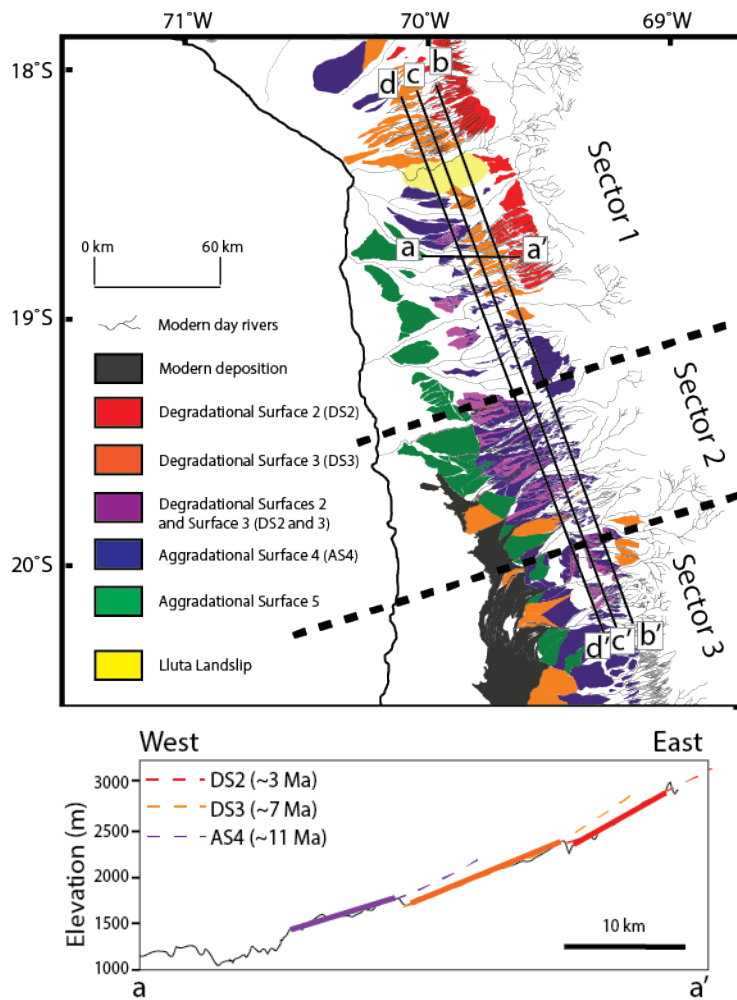
864 **10. Figures**



866 **Figure 1;** a) Sketch of Central Andes showing the five morphotectonic provinces.
 867 The main sectors and the fluvial systems within them are highlighted showing
 868 catchment area (b) Cross section of main morphotectonic provinces, location shown
 869 in Figure 1A. Major tectonics features of the region (Garcia et al., 2004; Victor et al.,
 870 2004; Farías et al., 2005; Juez-Larre et al., 2010; Allmendinger and Gonzalez 2014;).
 871 Length of reach of the major Sectors (1-3) over the morphotectonic provinces are
 872 highlighted.

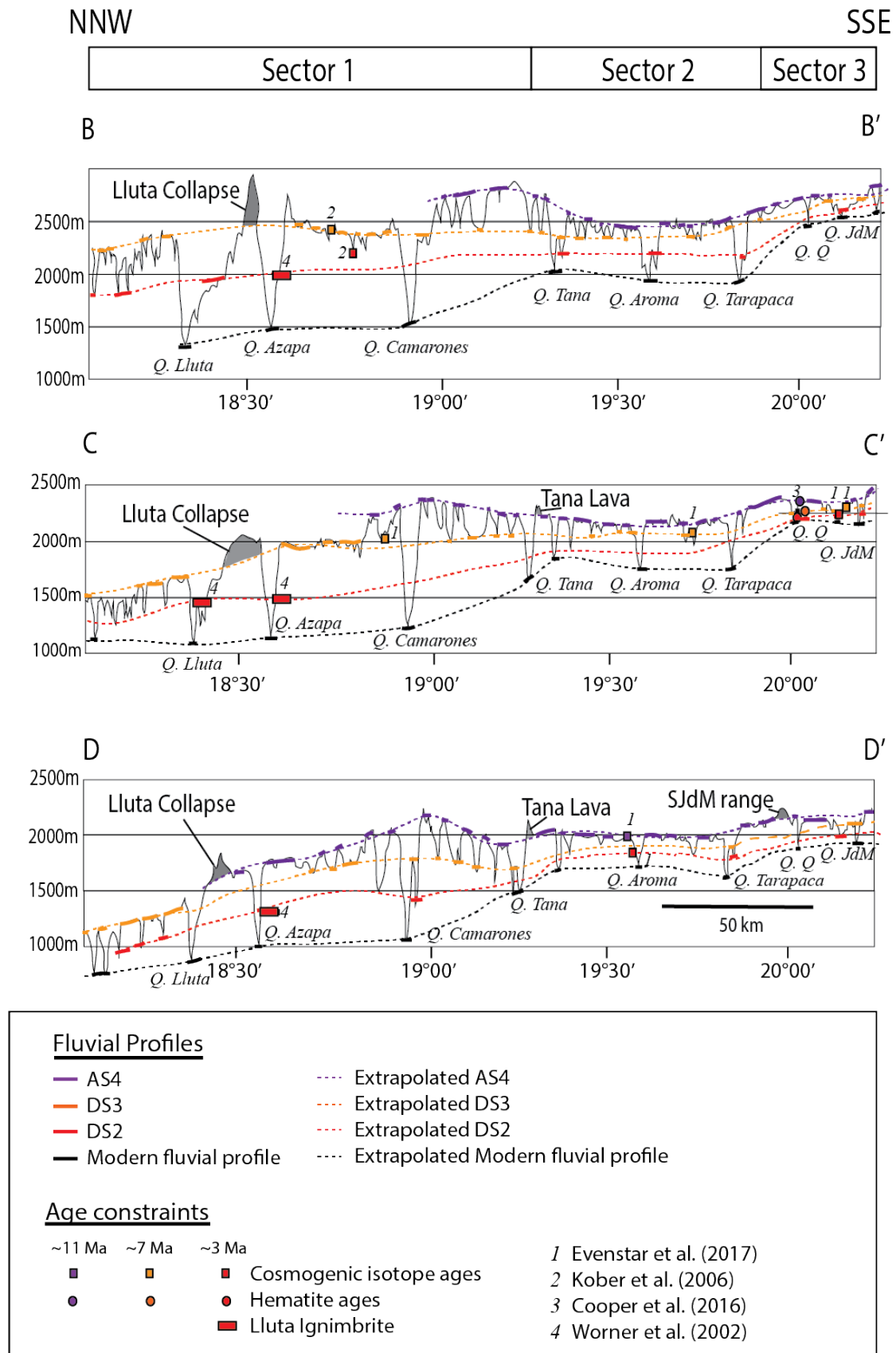


873
 874 **Figure 2;** (from left to right) Basic sedimentary overview of the Longitudinal Valley in
 875 the study area with the main geomorphic surfaces (AS5, AS4, DS3 and DS2).
 876 Climate profile for Longitudinal Valley (Jordan et al. 2014 and Evenstar et al. 2017)
 877 with timing for main geomorphic surfaces highlighted and timing of supergene
 878 minerals in Atacama (Aranciabia et al. 2009). Elevation profiles for Longitudinal
 879 Valley from Evenstar et al. 2015. Solid line represents Late Miocene uplift and
 880 dashed line Early Miocene uplift.



881

882 **Figure 3.** (Upper) Large scale map of Northern Chile showing the geomorphic
 883 surfaces (1-5) that form the Pacific Paleosurface (PPS). Black lines highlight the
 884 topographic cross sections (a-d) in figures 5. Black dashed lines separate regions of
 885 Sector 1-3. (Lower) Profile A shows a profile taken west to east across the
 886 Longitudinal Valley showing increasing incision of the paleosurfaces to the east
 887 through time.



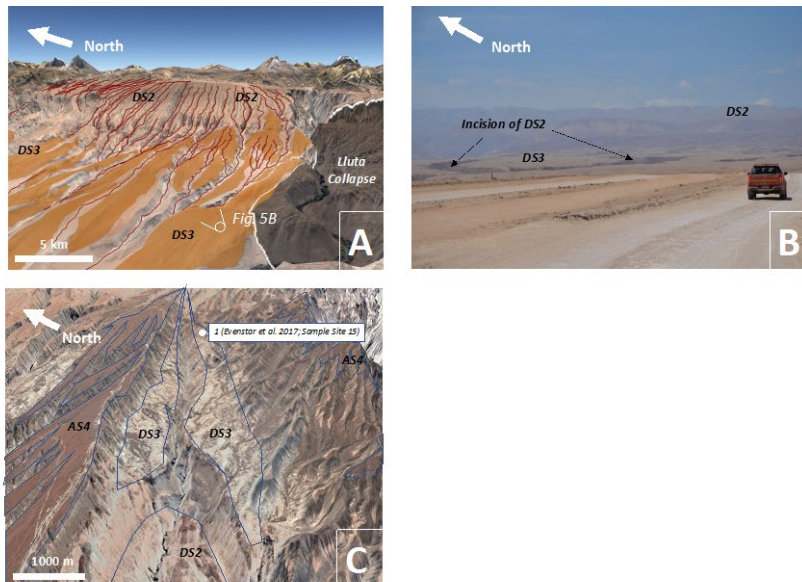
888

889 **Figure 4;** Three cross sections across the region. Locations shown in figure 3.

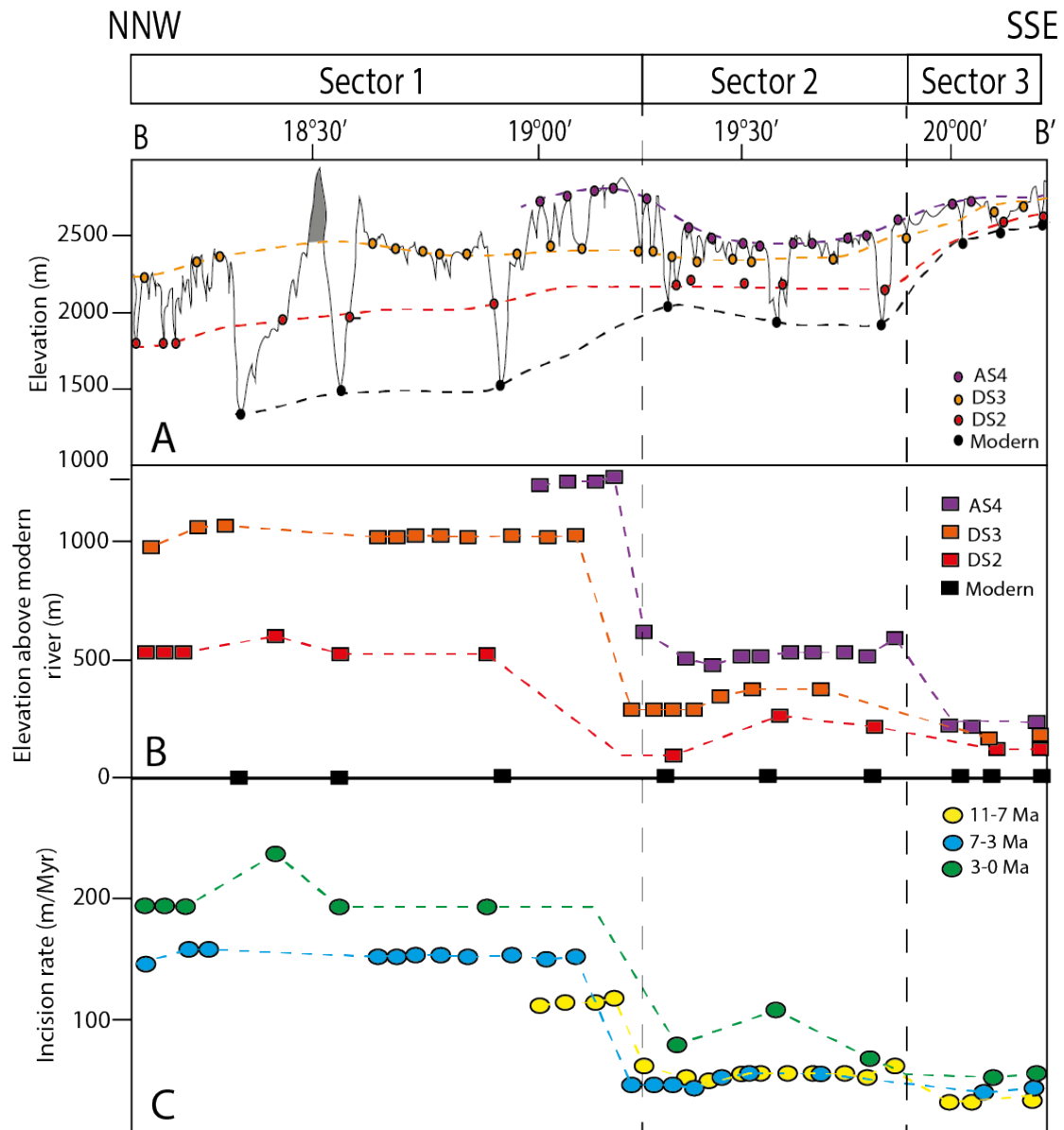
890 Profiles b-d are taken NNW to SSE. Black lines shows the topographic cross

891 sections across the region. Solid colour lines show the preserved parts of the surface

892 with the coloured dashed lines highlight the reconstructed paleo fluvial profiles
893 associated with each surface (AS 4, DS3, DS2 and the modern). Grey areas
894 represent anomalies on the topography profile. Key shows the main features that
895 control the age of the surfaces.

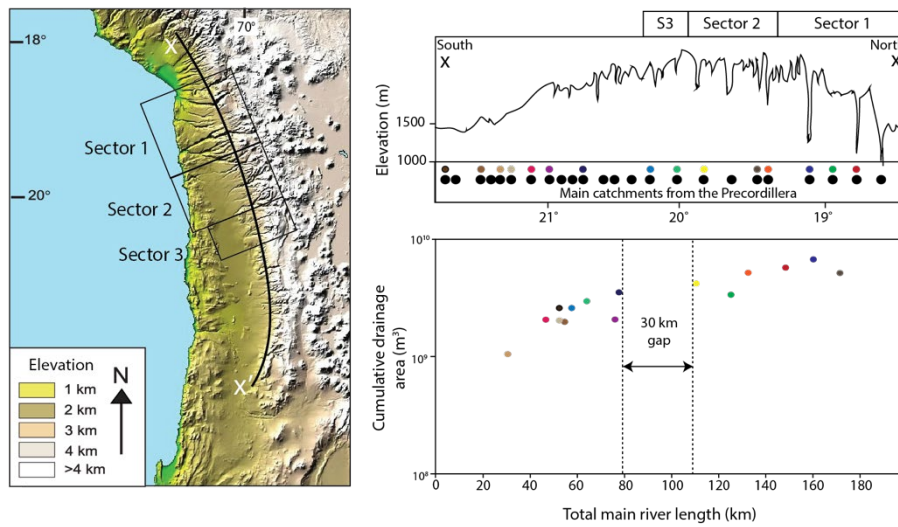


896
897 **Figure 5;** A) Google Earth image with 3x vertical exaggeration of DS2 cutting into
898 DS3, leaving DS3 as a series of relict inselberg highs north of Quebrada Lluta.
899 Location of photo of Figure 5B shown, B) Photo of same view taken from the field
900 showing incision of DS3 by DS2 C) Google Earth image with 3x vertical exaggeration
901 of DS3 and DS2 cutting into AS4 forming a lower terrace in Quebrada Camarones
902 with site location of *insitu* exposure age dating in Evenstar et al. 2017.



903

904 **Figure 6; A-** Cross section B showing the different paleo fluvial surfaces draped over
 905 an elevation profile. Coloured dots represent locations where the elevation was takes
 906 for Figure 6 B-C. **B** Shows the difference between paleo fluvial surfaces and modern
 907 fluvial profiles. **C** Incision rate through time calculated using the difference in
 908 elevation between the paleo fluvial surfaces and modern fluvial system divided by
 909 age of paleo fluvial surface.



910

911 **Figure 7;** (Top) Elevation profile along the eastern edge of the Longitudinal Valley
 912 from Evenstar et al., 2017 highlighting study area (Sector 1, Sector 2 and Sector 3
 913 (S3)). At the base of the elevation profile the black dots show the main fluvial
 914 systems from the Precordillera (the coloured dots relate to the dots in the cumulative
 915 drainage area graph below). (Bottom) cumulative drainage area of studied fluvial
 916 systems against length of fluvial system, this data was initially presented in Hoke et
 917 al. 2007 (supplementary material). a summary of cumulative drainage areas and
 918 fluvial length (distance from mouth) (Supplementary material in Hoke et al. 2007
 919 which have been combined and summarized in this paper)

920

921

922

923

924